Preprints of the 23rd IFAC World Congress
Busan, Republic of Korea, August 23-28, 2026

Loop-Element Sequence Selection for Reset Control Systems Under Multi-Frequency Reset Input ⋆

Ali Hosseini * **Sanjay Sivakumar** ** **Luke F. van Eijk** *,*** **Dragan Kostić** *** **Hassan HosseinNia** *

* *Department of Precision and Microsystems Engineering, Delft University of Technology, 2628 CD Delft, The Netherlands (e-mail: (s.a.hosseini, s.h.hosseinniakani)@tudelft.nl).*
** *ASMPT, 2 Yishun Ave 7, Singapore 768924 (e-mail: s.sivakumar@asmpt.com).*
*** *ASMPT, 6641 TL Beuningen, The Netherlands (e-mail: (luke.van.eijk, dragan.kostic)@asmpt.com).*

Abstract: This study develops a frequency-domain design framework for sequencing reset and linear elements in feedback loops subject to multi-frequency inputs. While Higher-Order Sinusoidal-Input Describing Functions (HOSIDFs) in existing reset-control studies assume single-frequency inputs and pure sinusoidal excitation, the proposed framework explicitly accounts for the reset element's input signal shaped by multiple sources of inputs. The method provides practical sequencing rules to reduce HOSIDFs while preserving the desired first-harmonic behavior. Design guidelines are formulated to minimize the closed-loop error while preserving the benefits of reset control over linear time-invariant designs. The effectiveness and practicality of the approach are demonstrated on an industrial wire bonding machine.

Keywords: Precision motion control, Reset control systems, Nonlinearity reduction.

1. INTRODUCTION

The main drawback of linear time-invariant (LTI) controllers is that they are subject to fundamental limitations, such as the waterbed effect and Bode's gain–phase relationship, as discussed in Freudenberg et al. (2000); Seron et al. (2012). It has been shown that these limitations can be relaxed by using reset elements (Clegg, 1958; Beker et al., 2004; Guo et al., 2009).

In Guo et al. (2009), reset elements are analyzed in the frequency domain using the sinusoidal-input describing function (SIDF). Building on this, Saikumar et al. (2021) and van Eijk et al. (2025) extend the framework to the Higher-Order SIDF (HOSIDF) and introduce a method for relating open-loop behavior to closed-loop dynamics in the frequency domain for reset controllers. Since reset elements are typically combined with LTI filters within the loop (see Fig. 1), their placement plays an important role in the resulting HOSIDFs, which are generally undesirable as they correspond to higher-order harmonics in the closed-loop response.

Several studies have therefore employed the HOSIDF framework to shape these higher-order harmonics while keeping the fundamental SIDF either unchanged or within a prescribed range. Cai et al. (2020) demonstrate that, by carefully selecting the sequence of loop components, the influence of HOSIDFs can be reduced without affecting the fundamental SIDF. Additionally, in Karbasizadeh and HosseinNia (2022) and Hosseini et al. (2025), a pre- and post-filtering approach is proposed that preserves the first-order harmonic response of the reset control system (RCS) while enabling the shaping of HOSIDFs.

However, all suggestions and conclusions in the aforementioned studies are derived for single-frequency input cases. That is, they assume that the input to the reset element is a pure sinusoidal signal, which is rarely the case in practical applications. Consequently, a gap remains in reset control design regarding how to select the optimal sequence of loop elements to achieve minimal closed-loop error for multi-frequency input cases. To address this gap:

- We propose a design framework for the placement and sequencing of loop elements in RCSs subject to multi-frequency reset input signals.

As mentioned earlier, the motivation for this work arises from practical applications in which the reset input signal is influenced by multiple sources, such as the reference $r \in \mathbb{R}$, disturbance $d \in \mathbb{R}$, and measurement noise $n \in \mathbb{R}$, as illustrated in Fig. 1. Thus, in this work:

- We study and validate the practicality of the proposed loop-element sequencing method on an industrial precision motion stage.

The remainder of this paper is organized as follows. Section 2 provides preliminaries on RCSs. Section 3 studies the effect of multi-frequency inputs on the reset element

⋆ This work is co-financed by ASMPT and Holland High Tech, Topsector High Tech Systems and Materials, with a PPS innovation grant public-private collaboration for research and development.

©2026 the authors. Accepted by IFAC for publication under a Creative Commons Licence CC-BY-NC-ND

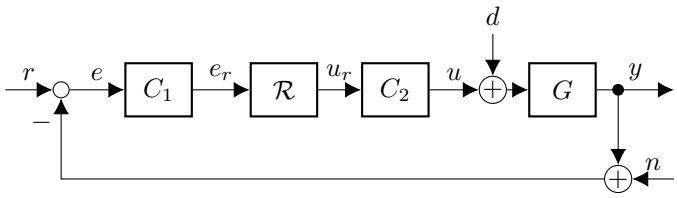


Fig. 1. Block diagram of the closed-loop system.

and presents the proposed design framework. In Section 4, the proposed method is validated through an industrial case study. Finally, Section 5 concludes the paper and outlines directions for future research.

2. PRELIMINARIES

2.1 System description

We consider the feedback architecture shown in Fig. 1. The LTI plant is denoted by G, while C_1 and C_2 correspond to LTI filters. The nonlinear component in the loop is a reset element, denoted by $\mathcal{R}$, whose dynamics are given by

$$\mathcal{R}: \begin{cases} \dot{x}_r(t) = A_r x_r(t) + B_r e_r(t), & (x_r(t), e_r(t)) \notin \mathcal{F}, \\ x_r(t^+) = A_\rho x_r(t), & (x_r(t), e_r(t)) \in \mathcal{F}, \\ u_r(t) = C_r x_r(t) + D_r e_r(t), \end{cases} \tag{1}$$

where the reset set $\mathcal{F}$ is defined as

$$\mathcal{F} := \{e_r = 0 \wedge (A_\rho - I)x_r(t) \neq 0\}. \tag{2}$$

The matrices $A_r \in \mathbb{R}^{n_r \times n_r}$, $B_r \in \mathbb{R}^{n_r \times 1}$, $C_r \in \mathbb{R}^{1 \times n_r}$, and $D_r \in \mathbb{R}$ define the underlying linear dynamics of the reset element. The matrix $A_\rho = \text{diag}(\gamma_1, \ldots, \gamma_{n_r})$, with $\gamma_i \in [-1, 1]$ for all $i \in \{1, \ldots, n_r\}$, specifies the post-reset scaling of each state. The state vector is denoted by $x_r(t) \in \mathbb{R}^{n_r}$, while $x_r(t^+) \in \mathbb{R}^{n_r}$ denotes the state immediately after a reset occurs. The signals $e_r(t) \in \mathbb{R}$ and $u_r(t) \in \mathbb{R}$ represent the input and output of the reset element, respectively. If the reset action is disabled, i.e., the element operates purely as an LTI system, the corresponding transfer function, referred to as the base linear system (BLS), is given by

$$R(s) = C_r(sI - A_r)^{-1}B_r + D_r, \tag{3}$$

with $s \in \mathbb{C}$ the Laplace variable.

2.2 Open-loop and Closed-loop Frequency Domain Analysis

The periodic response of a reset element subject to a sinusoidal input can be characterized through its harmonic decomposition. As established in Saikumar et al. (2021, Theorem 3.1), when the reset element is stimulated by a sinusoid $e_r(t) = \sin(\omega t)$, with $\omega \in \mathbb{R}$ as the input frequency, its output admits the harmonic expansion

$$u_r(t) = \sum_{n=1}^{\infty} |H_n(\omega)| \sin\left(n\omega t + \angle H_n(\omega)\right), \tag{4}$$

where the terms $H_n(\omega)$ represent the HOSIDFs associated with the state-space realization in (1) as follows

$$H_n(\omega) = \begin{cases} C_r \left(j\omega I - A_r\right)^{-1} \left(I + j\Theta_{\text{D}}(\omega)\right) B_r + D_r, \\ \qquad\qquad \text{for } n = 1, \\ C_r \left(jn\omega I - A_r\right)^{-1} j\Theta_{\text{D}}(\omega) B_r, \\ \qquad\qquad \text{for odd } n \geq 2, \\ 0, \qquad\qquad \text{for even } n \geq 2, \end{cases} \tag{5}$$

with $j^2 = -1$, and auxiliary matrices defined by

$$\begin{aligned} &\Lambda(\omega) = \omega^2 I + A_r^2, \qquad \Delta(\omega) = I + e^{\frac{\pi}{\omega}A_r}, \\ &\Delta_r(\omega) = I + A_\rho e^{\frac{\pi}{\omega}A_r}, \quad \Gamma_r(\omega) = \Delta_r^{-1}(\omega) A_\rho \Delta(\omega) \Lambda^{-1}(\omega), \\ &\Theta_{\text{D}}(\omega) = -\frac{2\omega^2}{\pi} \Delta(\omega) \left[\Gamma_r(\omega) - \Lambda^{-1}(\omega)\right]. \end{aligned} \tag{6}$$

Building on this result and using Caporale et al. (2024, Theorem 2), the open-loop higher-order frequency response of the architecture shown in Fig. 1 follows as

$$\mathcal{L}_n(\omega) = G(jn\omega) C_2(jn\omega) H_n(\omega) C_1(j\omega) e^{j(n-1)\angle C_1(j\omega)}. \tag{7}$$

Theorem 1, adapted from Saikumar et al. (2021), develops a frequency-domain-based approach for estimating closed-loop behavior of RCSs.

Theorem 1. (Saikumar et al., 2021, Theorem 4.1) Under the sinusoidal reference $r(t) = r_o \sin(\omega t)$ (with $r_o = 1$ since the reset element does not exhibit amplitude-dependent nonlinearities) and assuming Assumptions 1-3 in Saikumar et al. (2021) hold, the steady-state tracking error admits the decomposition

$$e_{ss}(t) = \sum_{n=1}^{\infty} e_n(t), \tag{8}$$

where each harmonic contribution is given by

$$e_n(t) = |S_n(\omega)| \sin\left(n\omega t + \angle S_n(\omega)\right), \tag{9}$$

and the higher-order sensitivity functions are

$$S_n(\omega) = \begin{cases} \dfrac{1}{1 + \mathcal{L}_1(\omega)}, & \text{for } n = 1, \\ -\mathcal{L}_n(\omega) S_{\text{bl}}(jn\omega) \left(|S_1(\omega)| e^{jn\angle S_1(\omega)}\right), & \\ \qquad\qquad \text{for odd } n \geq 2, \\ 0, \qquad\qquad \text{for even } n \geq 2, \end{cases} \tag{10}$$

with $S_{\text{bl}}(s) = \frac{1}{1 + L_{\text{bl}}(s)}$, where $L_{\text{bl}}(s)$ denotes the base linear open-loop transfer function.

The relevance and practicality of Assumptions 1–3 in Saikumar et al. (2021) are discussed in detail in Hosseini et al. (2026, Assumptions 1 and 2, Section II-C). Since we will later directly employ the reset controller designed in Hosseini et al. (2026), we do not repeat this discussion here and instead refer the reader to Hosseini et al. (2026) for a detailed justification of these assumptions.

It is straightforward from Theorem 1 to write

$$e_r(t) = \sum_{n=1}^{\infty} |S_{n,e_r}(\omega)| \sin\left(n\omega t + \angle S_{n,e_r}(\omega)\right), \tag{11}$$

with $S_{n,e_r}(\omega) = S_n(\omega) C_1(jn\omega)$. We then present the pseudo-sensitivity for e_r, as (van Eijk et al., 2025):

$$|S_{\infty,e_r}(\omega)| = \frac{\max\limits_{0 \leq t < 2\pi/\omega} |e_r(\omega, t)|}{r_o}. \tag{12}$$

3. OPTIMAL POSITION OF THE RESET ELEMENT IN THE LOOP UNDER MULTI-FREQUENCY EXCITATION

It is well established that when a nonlinear element is present in a feedback loop, its placement relative to the surrounding LTI components is critical, as different orderings yield different levels of nonlinearity (Cai et al., 2020; Karbasizadeh and HosseinNia, 2022). Prior work has suggested that, since in the HOSIDF expression in (7), C_1 appears as $C_1(j\omega)$ whereas C_2 appears as $C_2(jn\omega)$, one should strategically partition the loop's LTI dynamics between these two locations so as to minimize the generated HOSIDFs at the frequencies of interest. To quantify the resulting nonlinear behavior, the robustness factor σ_2 was introduced in Hosseini et al. (2025, Definition 2), where σ_2 quantifies the power of the higher-order harmonics in the error signal relative to the power of the first-order harmonic. We therefore propose the following loop-element placement strategy to minimize the impact of HOSIDFs:

- For each candidate sequence of linear and reset elements in the loop, compute $\sigma_2(\omega)$ as given in Hosseini et al. (2025, Lemma 1):

$$\sigma_2(\omega) = \frac{\sqrt{\sum_{n=1}^{\infty} |S_n(\omega)|^2} - |S_1(\omega)|}{|S_1(\omega)|}, \tag{13}$$

  and select the configuration that yields the smallest $\sigma_2(\omega)$ over the desired frequency range.

However, these results and associated conclusions rely on the assumption of a single-frequency sinusoidal input to the closed-loop system. In what follows, we therefore examine how the presence of an additional small-amplitude input at a frequency different from the primary excitation affects the resulting HOSIDFs and, consequently, the assessment of the reset element's optimal position.

To investigate the effect of this additional frequency component, we consider a Clegg integrator (CI) with $A_r = 0$, $B_r = 1$, $C_r = 1$, $D_r = 0$, and $\gamma = 0$. We first excite the CI with a sinusoidal signal

$$e_{r_1}(t) = \sin(2\pi f_1 t), \quad f_1 = 1 \text{ Hz},$$

and denote the corresponding output by $u_{r_1}(t)$. We then consider a second input of the form

$$e_{r_2}(t) = \sin(2\pi f_1 t) + 0.1\sin(2\pi f_2 t + \phi), \tag{14}$$

where $f_2 = 10$ Hz and the phase $\phi = 1.48\pi$ is independently drawn from the uniform distribution $\phi \sim \mathcal{U}[0, 2\pi)$. The output in this case is denoted by $u_{r_2}(t)$. Fig. 2 shows the reset output for these two inputs. As can be seen, there is a small difference in the reset times between the two cases. To better highlight this effect, the power spectral densities (PSDs) of $u_{r_1}(t)$ and $u_{r_2}(t)$ are shown in Fig. 3. Although (5) states that the reset element does not generate even harmonics, we observe that, for the input e_{r_2}, even harmonics are present because the input signal is no longer a single-frequency sinusoid.

This observation suggests that, since the reset signal in a closed-loop control system is never purely sinusoidal, the prefilter C_1 should be chosen such that the reset signal has most of its energy concentrated at a specific frequency. In this way, the reset signal e_r more closely resembles a pure sinusoidal signal, thereby avoiding the generation of additional nonlinear effects and higher-order harmonics. We therefore propose the following loop-element placement strategy for systems subject to multi-frequency inputs:

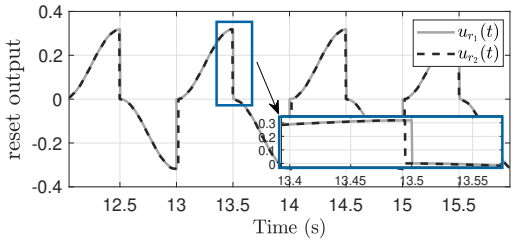


Fig. 2. Time-domain response of the Clegg integrator for the inputs $e_{r_1}(t)$ and $e_{r_2}(t)$.

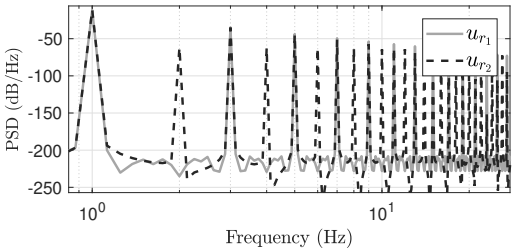


Fig. 3. The PSD of the reset output signal.

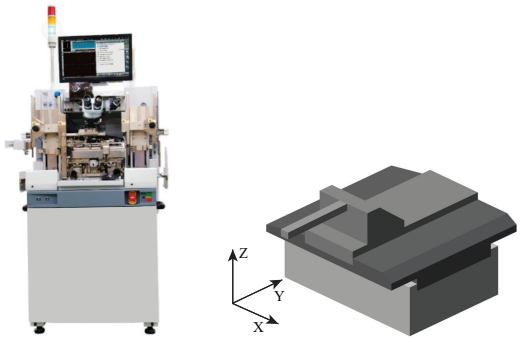
- Given an LTI closed-loop control system, perform the PSD analysis of the error signal to identify the dominant frequency component (denoted by ω_{p_1}) and the remaining $k-1$ non-dominant frequency components (denoted by ω_{p_i} for all $i \in \{2, \ldots, k\}$).
- Subsequently, follow all the steps described in (Hosseini et al., 2026, Section V.A) to design a reset controller that improves the performance of the existing LTI controller, specifically at ω_{p_1}.
- Let $E(\omega)$ denote the PSD of the measured error under the LTI controller. We then estimate the PSD of the reset input signal e_r as

$$|E_r(\omega)| \approx \frac{|S_{\infty,e_r}(\omega)|}{|S(j\omega)|}\, E(\omega), \tag{15}$$

  where $S(j\omega)$ is the sensitivity function (e/r) of the LTI system. The relation in (15) is straightforward to derive by expressing the reference signal as $|R(\omega)| = \frac{|E(\omega)|}{|S(j\omega)|}$ for the LTI controller, and, in the RCS case, approximately as $|R(\omega)| \approx \frac{|E_r(\omega)|}{|S_{\infty,e_r}(\omega)|}$. Equating these two expressions for $|R(\omega)|$ directly yields (15).
- Having the vector $v = \left[E_r(\omega_{p_2}), \ldots, E_r(\omega_{p_k})\right]^\top$ containing the PSD values at all non-dominant vibration frequencies ω_{p_i}, $i \geq 2$, we define the metric Δ_{E} as

$$\Delta_{\mathrm{E}} = \frac{\|v\|_p}{|E_r(\omega_{p_1})|} \times 100, \tag{16}$$

  where $\|\cdot\|_p$ denotes an arbitrary vector norm (e.g., an ℓ_p-norm with $p \in [1, \infty]$). The metric Δ_{E} quantifies the relative contribution of the non-dominant vibration components to the reset input; alternative application-specific metrics (e.g., phase-dependent metrics) may also be used.
- Based on the selected norm, we compute Δ_{E} for each candidate sequence of LTI elements in C_1 and C_2 (as



(a) (b)

Fig. 4. (a) The industrial wire bonder. (b) The schematic representation of the XYZ stages.

their building blocks, e.g., lead, lag, notch, ...). At this stage, the designer may specify a threshold on Δ_{E}, and any candidate for which Δ_{E} exceeds this threshold is discarded. In this study, for robustness, we set this threshold to 10% for the ℓ_∞ norm.

- Finally, we compute $\sigma_2(\omega)$ for each remaining candidate and select the one that yields the smallest $\sigma_2(\omega)$ over the desired frequency range. This ensures that the selected sequence achieves the lowest HOSIDFs among all sequences satisfying the Δ_{E} threshold.

Please note that the 10% threshold on Δ_{E} is specific to this use case. Based on our measurements, the considered motion stage does not operate robustly above this value; however, this threshold may differ for other systems. Building on the sequencing procedure outlined above, the next section presents a case study of an RCS for an industrial motion platform, demonstrating the importance of the chosen loop-element sequence.

4. EXPERIMENTAL RESULTS

In this section, we consider the industrial wire bonder presented in Fig. 4 as a case study. A wire bonder (see Fig. 4a) is a machine that connects conducting wires between an integrated circuit and its packaging, forming a microchip. Its motion platform has three degrees of freedom, controlled in Cartesian coordinates. A simplified schematic of the XYZ stages of the wire bonder is shown in Fig. 4b, including the base frame that isolates vibrations between the motion stages and the environment. Each axis is driven by a dedicated actuator and, within the operating range, each motion axis can be modeled as a Single-Input Single-Output (SISO) LTI system.

In this study, we focus on the motion control of the wire bonder's X-stage, where its measured frequency response function is denoted as G. A typical X-direction reference profile is shown in Fig. 5 and consists of three phases: a tracking phase, where the end-effector moves between bonding locations; a settling phase, allowing residual vibrations to decay; and a final bonding phase, during which the actual wire bond is formed. Surrounding the reference signal are permissible error bounds for the end-effector. These bounds are essential to avoid unintended contact with previously bonded wires or nearby structures during the tracking and settling phases. Additionally, we define

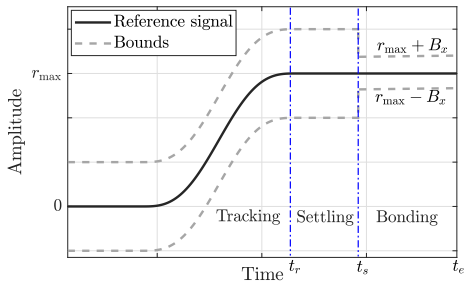


Fig. 5. Typical reference signal profile in the X-direction, divided into the tracking, settling, and bonding phases. The indicated bounds are exaggerated.

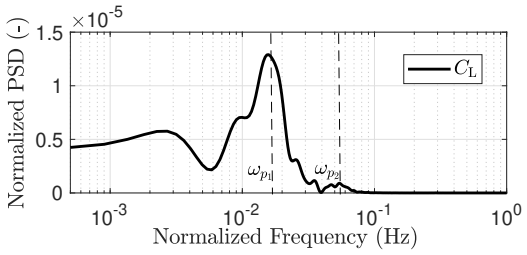


Fig. 6. The PSD of the measured error (for C_{L}) during the forward motion in the settling and bonding phases.

the settling time of the system as the last time the position of the end-effector is located outside the $r_{\max} \pm B_{\mathrm{x}}$.

In Hosseini et al. (2026), an automatically tuned LTI controller (C_{L}) is considered to push performance to the limits of linear control. The controller aims to achieve optimal tracking performance, maximizing the bandwidth while increasing the loop gain, and simultaneously satisfying the robustness conditions as

$$M_{\mathrm{s}} \leq 6\,\mathrm{dB}, \quad M_{\mathrm{r}} \leq 2.5\,\mathrm{dB}, \tag{17}$$

where $M_{\mathrm{s}} = \max_{\omega<\omega_{\mathrm{res}}} |S(j\omega)|$, with $S(j\omega) = 1/\left(1 + C_{\mathrm{L}}(j\omega)G(j\omega)\right)$ being the sensitivity function. Also, $M_{\mathrm{r}} = \max_{\omega\geq\omega_{\mathrm{res}}} |S(j\omega)|$, where $\omega_{\mathrm{res}} \in \mathbb{R}_{>0}$ denotes the frequency prior to the first resonance or anti-resonance of the plant. The PSD of the error signal in the forward motion (during settling and bonding region) is shown in Fig. 6. Please note that, for confidentiality reasons, all frequency axes in the wire bonder experiments have been normalized with respect to the Nyquist frequency. However, it is worth noting that the sampling frequency used in the experimental implementation is on the order of 10 kHz. A dominant problematic frequency component is identified at ω_{p_1}. Accordingly, the reset controller C_{NL_1} is designed to preserve the prescribed robustness margins while attenuating vibrations around ω_{p_1}. Although ω_{p_2} is not directly problematic in terms of the error signal, it may introduce additional frequency components in the reset signal, potentially leading to undesired reset actions.

Since the details of the controller synthesis and parameter tuning are beyond the scope of this study, we adopt the two controllers (C_{L} and C_{NL_1}) from Hosseini et al. (2026). Fig. 7 depicts the open-loop frequency responses, $L_{\mathrm{linear}}(j\omega) = C_{\mathrm{L}}(j\omega)G(j\omega)$ for the LTI controller and $\mathcal{L}_1(\omega)$ for the reset-based controller. The reset-based controller aims to address vibrations around ω_{p_1} by increasing

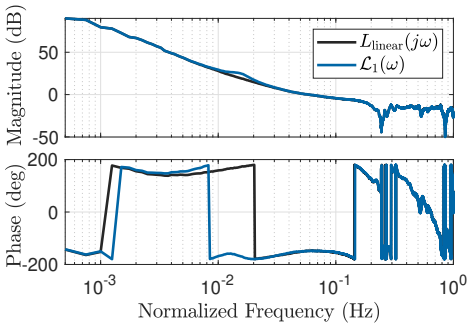


Fig. 7. Open-loop frequency responses of the linear and reset-based controllers.

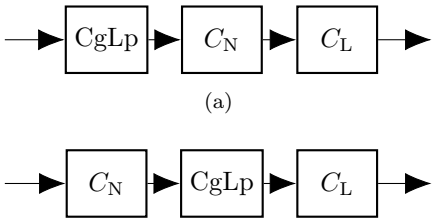


Fig. 8. The reset-based controller structures (a) Sequence 1, (b) Sequence 2.

the loop gain while preserving the phase margin at the gain crossover frequency. The latter is achieved by employing a Constant-in-Gain, Lead-in-Phase (CgLp)-based controller, which provides a positive phase contribution around the targeted bandwidth while maintaining an approximately unity gain (see Hosseini et al. (2026, Definition 1)). The expression $\mathcal{L}_n(\omega)$ in (7) shows that $\mathcal{L}_1(\omega)$ is invariant to the placement of the loop elements. Consequently, the $\mathcal{L}_1(\omega)$ in Fig. 7 remains unchanged regardless of the placement of the reset element within the loop.

In the following, we demonstrate how to determine the optimal placement of the loop elements for the reset-based controller C_{NL_1}, as outlined in Section 3. The controller C_{NL_1} consists of the LTI controller C_{L}, an inverse notch filter C_{N}, and a CgLp element. The CgLp element itself comprises a Generalized First-Order Reset Element (GFORE) (Guo et al., 2009) and a lead filter; however, for ease of exposition, we treat it as a single block. Furthermore, we keep the location of the LTI controller C_{L} fixed, because it is an auto-tuned higher-order controller and the firmware of the considered wire bonder does not allow arbitrary placement of such a higher-order controller within the loop. Fixing the location of C_{L} and treating the CgLp element as a single block, therefore, yields two distinct loop-element sequences for the nonlinear controller, as illustrated in Fig. 8.

To select which sequence should be used, a common practice, as mentioned in Section 3, is to assess the level of nonlinearity and select the controller that generates lower HOSIDFs. Accordingly, the robustness factor $\sigma_2(\omega)$ is computed for both configurations and depicted in Fig. 9. From this figure, Sequence 1 is expected to generate lower HOSIDFs than Sequence 2; hence, based solely on HOSIDF reduction, Sequence 1 would appear preferable.

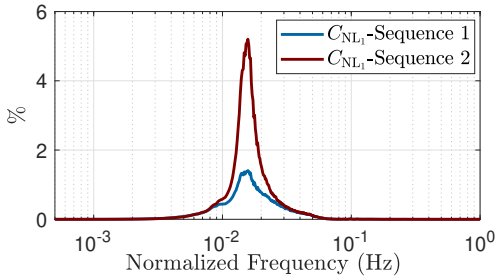


Fig. 9. Robustness factor $\sigma_2(\omega)$ (in %) for C_{NL_1} under Sequence 1 and Sequence 2 configurations.

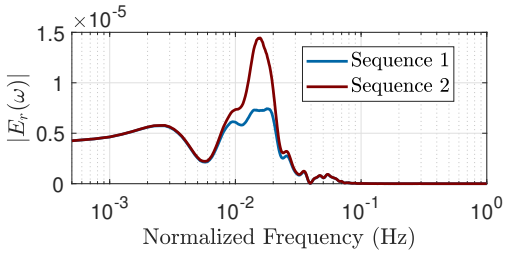


Fig. 10. $|E_r(\omega)|$ for Sequence 1 and Sequence 2.

However, we have shown that, in the presence of multi-frequency reset inputs, this design procedure can be inaccurate. Therefore, for loop-element sequence selection, we instead follow the steps outlined in Section 3. The first two steps have already been completed: the problematic frequency ω_{p_1} has been identified, and an appropriate reset controller C_{NL_1} has been designed. For the two candidate configurations, $|E_r(\omega)|$ is computed and plotted in Fig. 10. This quantity represents the estimated PSD of the reset input signal inferred from the measurements.

We then evaluate Δ_{E} for both sequences using the ℓ_∞ norm, resulting in 12.6% for Sequence 1 and 6.4% for Sequence 2. Since, in this study, we set the threshold to $\Delta_{\text{E}} = 10\%$, Sequence 1 is discarded. The analysis therefore indicates that Sequence 2 should be selected, as it is expected to yield better performance by concentrating a larger portion of the reset-input power at the dominant vibration frequency (lower Δ_E).

To illustrate the resulting performance, the time-domain error and the corresponding cumulative PSD for C_{L}, and for C_{NL_1} with Sequence 1 and Sequence 2, are shown in Fig. 11. Relative to the linear controller, Sequence 1 and Sequence 2 yield approximately 12% and 74% reductions in settling time, and about 43% and 61% reductions in the root-mean-square (RMS) error, respectively.

The improvement achieved with Sequence 2 is solely due to the careful placement of the loop components around the nonlinear element. To better understand how Sequence 2 leads to such an improvement, Fig. 12(a) and (c) show the input and output of the reset element ($e_r(t)$ and $u_r(t)$) for both sequences. It can be observed that, since Sequence 2 is designed to yield a smoother reset signal dominated by a single frequency component, the undesired excessive reset actions present in Sequence 1 are largely avoided, which in turn reduces the generation of higher-order harmonics. Furthermore, Fig. 12(b), which presents the PSD of the reset signal, indicates that Sequence 2 yields a reset signal

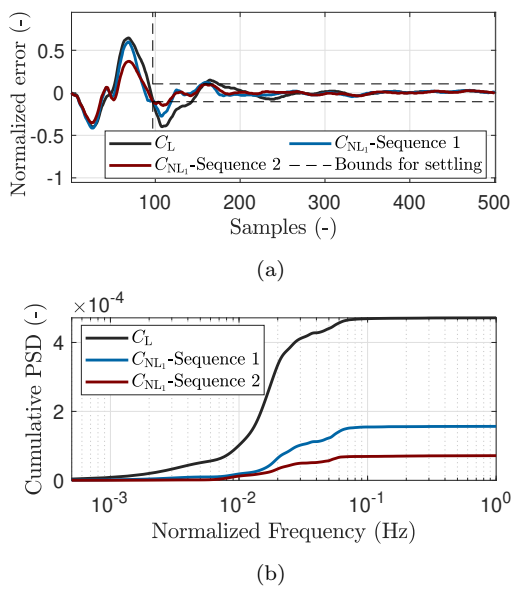


Fig. 11. (a) Normalized error signals for forward motion. (b) Cumulative PSD of the errors within the settling and bonding region (indicated by dotted line in (a)).

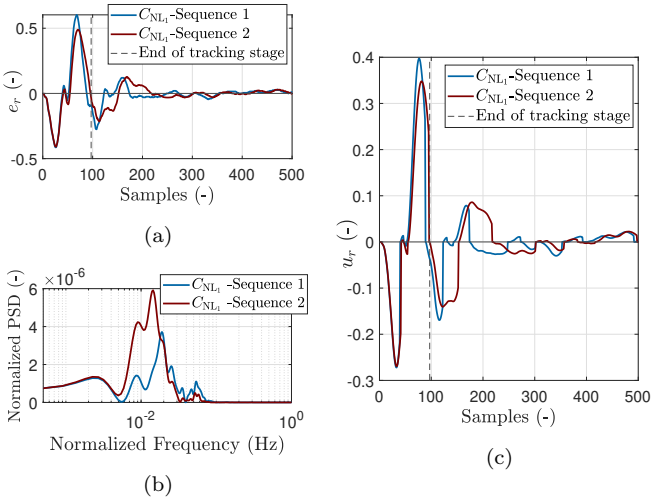


Fig. 12. (a) The measured input of the reset element ($e_r(t)$). (b) The PSD of the reset signal $e_r(t)$. (c) The measured output of the reset element $u_r(t)$.

whose energy is more strongly concentrated around ω_{p_1} and less spread over other frequencies.

This industrial case study demonstrates that HOSIDF-based loop-sequencing criteria can be misleading when the reset signal contains multiple frequency components rather than a pure sinusoid. We recommend selecting loop-element sequences that suppress frequency components in the reset signal, as the superposition principle does not hold in RCSs. This is because additional frequency components can induce undesired reset actions, stronger nonlinear effects, and ultimately suboptimal performance.

5. CONCLUSION

We demonstrated that, contrary to existing studies, there is no general optimal sequence of loop elements for RCSs. This is because the reset signal contains multiple frequency components, making a selection strategy based solely on HOSIDF reduction unreliable. To address this, we proposed a loop-element sequencing method that combines frequency-domain HOSIDF analysis with time-domain performance measurements. The effectiveness of the method was validated on an industrial motion stage, where a restructured RCS achieved a 70% reduction in settling time and a 31% reduction in RMS error with respect to the HOSIDF-based optimized reset controller. Future work will focus on designing band-pass nonlinear reset elements that confine the reset action to the desired operating region, ensuring operation within the targeted frequency band under multi-frequency excitation.

REFERENCES

Beker, O., Hollot, C., Chait, Y., and Han, H. (2004). Fundamental properties of reset control systems. *Automatica*, 40(6), 905–915.

Cai, C., Dastjerdi, A.A., Saikumar, N., and HosseinNia, S. (2020). The optimal sequence for reset controllers. In *Proc. Euro. Cont. Conf.*, 1826–1833.

Caporale, D., van Eijk, L.F., Karbasizadeh, N., Beer, S., Kostić, D., and HosseinNia, S.H. (2024). Practical implementation of a reset controller to improve performance of an industrial motion stage. *IEEE Trans. Control Syst. Technol.*, 32(4), 1451–1462.

Clegg, J.C. (1958). A nonlinear integrator for servomechanisms. *Trans. of the American Institute of Elec. Eng.*, 77(1), 41–42.

Freudenberg, J., Middleton, R., and Stefanpoulou, A. (2000). A survey of inherent design limitations. In *Proc. of American Cont. Conf.*, volume 5, 2987–3001.

Guo, Y., Wang, Y., and Xie, L. (2009). Frequency-domain properties of reset systems with application in hard-disk-drive systems. *IEEE Trans. Control Syst. Technol.*, 17(6), 1446–1453.

Hosseini, S.A., Kostić, D., and HosseinNia, S.H. (2025). Robust performance analysis and nonlinearity shaping for closed-loop reset control systems. *arXiv:2509.02143*.

Hosseini, S.A., Quinten, F.R., van Eijk, L.F., Kostić, D., and Hassan HosseinNia, S. (2026). Frequency-domain design of a reset-based filter: An add-on nonlinear filter for industrial motion control. *IEEE Transactions on Control Systems Technology*, 34(2), 919–933.

Karbasizadeh, N. and HosseinNia, S.H. (2022). Continuous reset element: Transient and steady-state analysis for precision motion systems. *Control Engineering Practice*, 126, 105232.

Saikumar, N., Heinen, K., and HosseinNia, S.H. (2021). Loop-shaping for reset control systems: A higher-order sinusoidal-input describing functions approach. *Control Engineering Practice.*, 11, 104808.

Seron, M.M., Braslavsky, J.H., and Goodwin, G.C. (2012). *Fundamental limitations in filtering and control.* Springer Science & Business Media.

van Eijk, L.F., Kostić, D., and Hassan HosseinNia, S. (2025). Frequency response analysis of general zero-crossing reset control systems. *IEEE Contr. Syst. Lett.*, 9, 1105–1110.